

Electron reorganization triggered by electron transfer: the inter-valence charge transfer of a $\text{Fe}^{3+}/\text{Fe}^{2+}$ bi-metallic complex

Alex Domingo*, Celestino Angeli†, Coen de Graaf‡§, Vincent Robert¶

October 14, 2014

Abstract

The key role of the molecular orbitals in describing electron transfer processes is put in evidence for the intervalence charge transfer (IVCT) of a synthetic non-haem binuclear mixed-valence $\text{Fe}^{3+}/\text{Fe}^{2+}$ compound. The electronic reorganization induced by the IVCT can be quantified by controlling the adaptation of the molecular orbitals to the charge transfer process. We evaluate the transition energy and its polarization effects on the molecular orbital by means of *ab initio* calculations. The resulting energetic profile of the IVCT shows strong similarities to the Marcus' model, suggesting a response behaviour of the ensemble of electrons analogue to that of the solvent. We quantify the extent of the electronic reorganization induced by the IVCT process to be 11.74 eV, a very large effect that induces the crossing of states reducing the total energy of the transfer to 0.89 eV.

Keywords: Electron Transfer, Transition Metal, Electronic Structure, Ab Initio, Molecular Orbitals. ■

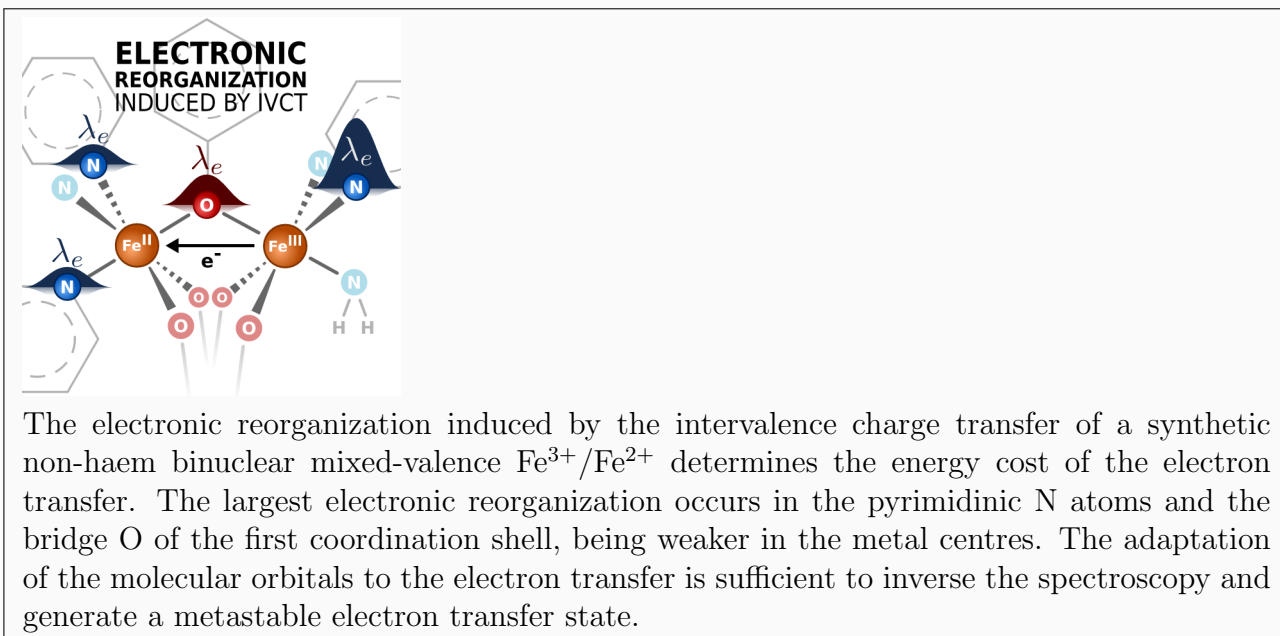
*Department of Chemistry, KU Leuven, Celestijnenlaan 200F, B-3001 Heverlee-Leuven, Belgium

†Dipartimento di Scienze Chimiche e Farmaceutiche, Università di Ferrara, via Fossato di Mortara 17, 44121 Ferrara, Italy

‡Departament de Química Física i Inorgànica, Universitat Rovira i Virgili, Marcel·lí Domingo s/n, 43007 Tarragona, Spain

§Institució Catalana de Recerca i Estudis Avançats (ICREA), Passeig Lluís Companys 23, 08010 Barcelona, Spain

¶Laboratoire de Chimie Quantique, Institut de Chimie UMR 7177, Université de Strasbourg, 4 rue Blaise Pascal, 67000 Strasbourg, France



INTRODUCTION

Energy conversion processes in biological systems usually rely on redox chemical reactions. Photo-synthesis,¹ respiration² and the DNA resistance to UV³ are prime examples of essential phenomena based on internal charge transfer. The same attribute holds true for the wealth of devices produced by molecular science, like fuel cells,^{4,5} chemical sensors^{6,7} or dye-sensitized solar cells.⁸ However, electron transfer in multi-electronic systems is fundamentally complex. The correlation effects existing between the particles turn the electron excitation into a collective phenomenon of the multi-electronic system. We present herein a wave function based strategy that offers a detailed description of the electronic response induced by the electron transfer on the electron cloud of the system. Such response can have dramatic effects on the electronic structure, being key in obtaining accurate energetics of the transfer reaction.

The Marcus-Hush-Levich theory for electron transfer reactions, usually referred as Marcus' theory,^{9,10} incorporates the reorganization induced in the environment of the transfer sites at a nuclear level. Even though the simplest electron transfer reactions do not imply any bond breaking or formation, they do induce charge reorganization in the environment of the hole and particle sites. Precisely, short- and long-range response effects will alter the electronic and nuclear structures of the surroundings to some extent. The region closest to the transfer sites forms the so-called inner-sphere model, which in the case of medium-sized molecules incorporates the intimate structures of reactants and products. The outer-sphere model surrounds the inner-sphere and is usually formed by solvent molecules. The structural changes undergone by these two regions have a major role on defining the energetic efficiency of the electron transfer process. **Figure 1** shows schematically the adiabatic potential energy surfaces of the donor (M_b) and acceptor (M_a) parts along the electron transfer of one unit of charge. The characteristics of the crossing between the two potential surfaces define the energetic profile of the transfer and ultimately, its efficiency.¹¹

Nature has found various strategies to minimize the energy penalty of displacing an electron from one region to another. One reported mechanism to avoid high-energy intermediates and charge accumulation consists in coupling the electron transfer to the migration of

a proton, the so-called proton-coupled electron transfer (PCET).^{12,13} In biology, such concerted processes can be illustrated by the abundant class of metalloproteins, which present a non-haem binuclear iron active site involved in the transport and activation of dioxygen.^{14,15} An outstanding example exhibiting such PCET phenomenon is the bio-mimetic compound $[\text{Fe}^{\text{III}}\text{Fe}^{\text{II}}(\text{NH}_2\text{-L})(\text{mpdp})]^{2+}$ (mpdp²⁻ stands for m-phenylenedipropionate).^{16,17} **Figure 2** illustrates the protonated structure of this particular bi-iron complex, which is referred as $\text{Fe}_a^{\text{III}}\text{Fe}_b^{\text{II}}\text{LH}$. The mixed-valence $\text{Fe}^{3+}/\text{Fe}^{2+}$ bimetallic core is subject to inter-valence charge transfer (IVCT), while the NH_2 group attached to the Fe_b^{II} centre is likely to be deprotonated.¹⁷ The proton transfer in NH_2 and the electron transfer between the Fe centres are coupled and can be triggered by a change of pH or by light radiation, for example. In any case, the PCET process of $\text{Fe}_a^{\text{III}}\text{Fe}_b^{\text{II}}\text{LH}$ follows a concerted mechanism,¹⁷ as it is the case for many other electrochemical reactions involving a PCET.^{18,19}

Since the coordination spheres of the two iron centres in $\text{Fe}_a^{\text{III}}\text{Fe}_b^{\text{II}}\text{LH}$ are almost identical, it is expected that the inter-metallic electron transfer step should exhibit a standard free energy value (ΔG^0) close to zero. Thus, the related kinetics and thermodynamics of these electron transfer reactions are mainly governed by the reorganization energy (λ) as defined in Marcus' theory (**Figure 1**). Along this picture, λ consists of two contributions arising from the inner and outer-spheres, which both involve the displacement of nuclei. On the other hand, the electrons of reactants and products can be considered apart from the inner and outer-spheres since their response to electronic excitations are much faster than those of the nuclei, typically of the order of sub-femtosecond to few femtoseconds.^{20,21} We call this electronic entity the electronic-sphere to make contact with Marcus' theory and we write $\lambda = \lambda_o + \lambda_i + \lambda_e$, where λ_o refers to the reorganization of the solvent (outer-sphere), λ_i to the vibrational reorganization (inner-sphere) and λ_e to the electronic reorganization (electronic-sphere). In this study we address the effect that λ_e has on λ . This particular contribution to λ explicitly depends on the quantity of charge transferred (Δe) and can be approximated by the energy of the inter-valence transition if Δe equals one unit of charge.

The evaluation of the IVCT transition energy is challenging for standard quantum chemistry methods (see Methods). We establish a bottom-up numerical strategy, based on electronic wave functions, that incorporates the adaptation of the full electronic structure to the

electron transfer state in the form of state-specific molecular orbitals (MO). Hence, by comparing the MOs of the states involved in the transition, it is possible to quantify and analyse the electronic reorganization induced by the inter-metallic charge transfer to all the electrons of the complex. This procedure allows one to evaluate λ_e , which is a critical quantity to obtain accurate estimates of the IVCT transition energy of the $\text{Fe}_a^{\text{III}}\text{Fe}_b^{\text{II}}\text{LH}$ complex.

METHODOLOGY

We use the molecular structure of the $\text{Fe}_a^{\text{III}}\text{Fe}_b^{\text{II}}\text{LH}$ derived from X-ray data,¹⁷ without performing any further computational geometrical refinement or chemical simplification. Since we focus exclusively on the fate of the electrons, we stay under the Born-Oppenheimer approximation with fixed atomic positions.^{22,23} The model of $\text{Fe}_a^{\text{III}}\text{Fe}_b^{\text{II}}\text{LH}$ employed comprises a single molecule isolated in the void. Even though the phenomenon of PCET is observed in water, the electron reorganization triggered by the IVCT is found to not extend significantly beyond the first coordination shell of the bi-metallic core, minimizing the impact of the solvent on such electronic response effects (see Results).

The size of $\text{Fe}_a^{\text{III}}\text{Fe}_b^{\text{II}}\text{LH}$ suggests to work with Density Functional Theory (DFT) based methods.²⁴ Charge transfer excitations in organic donor-acceptor systems have been computationally characterized within the time-dependent DFT framework,^{25–27} incorporating many-body Green’s function techniques and using the Bethe-Salpeter formalisms.²⁸ Nevertheless, the standard formalisms based on DFT fail to describe the electron-trapped mixed-valence state of the $\text{Fe}_a^{\text{III}}\text{Fe}_b^{\text{II}}\text{LH}$ compound. Due to a dominating Coulomb term, the resulting DFT charge distribution is artificially delocalized over the two metal centres independently of the functional employed.²⁹ Wu *et al.* developed the constrained DFT (C-DFT) method to overcome this specific shortcoming by including an *ad hoc* constraint to the electronic density in the Kohn-Sham procedure.^{30–32} In spite of the successful results achieved with C-DFT on various mixed-valence compounds,^{33,34} this strategy was not reliable to describe the electron-trapped mixed-valence state of the $\text{Fe}_a^{\text{III}}\text{Fe}_b^{\text{II}}\text{LH}$ complex, which we found to significantly depend on the arbitrary choice of the charge distribution constraint.

On the other hand, the *ab initio* complete active space self-consistent field (CASSCF)

method³⁵ produces the expected electron-trapped state ($\text{Fe}_a^{\text{III}}/\text{Fe}_b^{\text{II}}$) as the electronic ground state of the $\text{Fe}_a^{\text{III}}\text{Fe}_b^{\text{II}}\text{LH}$ compound. The CASSCF wave function is built upon all the possible configurations that can be composed over the so-called active space (CAS). Since the ground state of the $\text{Fe}_a^{\text{III}}\text{Fe}_b^{\text{II}}\text{LH}$ complex is dominated by the $\text{Fe}_a^{\text{III}}(3d^5)/\text{Fe}_b^{\text{II}}(3d^6)$ electronic configuration, we define a CAS formed by eleven electrons distributed over the ten $3d$ -like MOs of the two Fe centres, totalling a CAS[11,10]. This relatively small active space can generate the ground state as well as all the intra-metallic and inter-metallic electronic excitations. Notably, we describe the lowest energy IVCT state ($\text{Fe}_a^{\text{II}}/\text{Fe}_b^{\text{III}}$), the excited state participating in the intramolecular electron transfer process involved in the PCET of this compound.

Unfortunately, there is no systematic way to obtain a single state CASSCF wave function optimized for an excited state (as the IVCT) due to root-flipping problems during the optimization procedure. We devise a computational strategy that uses the state-average (SA) CASSCF result as starting point and gradually increases the weight of the IVCT excited state in the CASSCF orbital optimization, raising the degree of adaptation of the MO set to the IVCT state. The goal is to reach 100% of IVCT weight, the state-specific point where the MOs are fully adapted to the IVCT state. There are two factors that control the relative weight of a particular excited state in the MO optimization, one is the total number of electronic states and the other is the weight ratio defined between them. The former can be controlled by the size of the active space and the latter can be directly tuned by setting the weight ratio between the states that participate in the orbital optimization.

The starting SA-CASSCF calculation of the $\text{Fe}_a^{\text{III}}\text{Fe}_b^{\text{II}}\text{LH}$ compound is performed including eight states with a total spin value of $S = 9/2$. We work specifically with high-spin (HS) states to reduce the total number of possible states incorporated in the calculation. The splitting between the spin-states caused by the exchange coupling constant in this kind of bi-iron compounds is negligible compared to the energies of the electronic excitations.³⁶ The resulting eight HS states are three almost degenerate states corresponding to the ground state with a dominant configuration of the type $\text{Fe}_a^{\text{III}}(t_{2g}^3e_g^2)/\text{Fe}_b^{\text{II}}(t_{2g}^4e_g^2)$, two internal d-d transitions on either Fe_a^{III} or Fe_b^{II} and three almost degenerate IVCT states with a dominant configuration of the type $\text{Fe}_a^{\text{II}}(t_{2g}^4e_g^2)/\text{Fe}_b^{\text{III}}(t_{2g}^3e_g^2)$. For the sake of simplicity, we use the orbital

representations of the O_h point group, even though the environment of the metal centres is slightly distorted from the octahedral symmetry. At the SA-CASSCF level, the total weight of the IVCT state is solely $3/8 = 37.50\%$. From this point, the weight of the IVCT is increased to some arbitrary degree and one macro-iteration of the CASSCF is executed. Subsequently, the character of the resulting states is identified and the distribution of weights is readjusted in the case that root-flipping occurs. The CASSCF macro-iterations are repeated until convergence. Since each state is described with its own set of MOs, we performed a last step consisting in a state interaction calculation to ensure the orthogonality.³⁷ The current procedure is the last step of the work started by Domingo *et al.* to improve the description of metal-to-metal charge transfer states³⁸ and continued by Meyer *et al.*³⁹ The present work goes further though, resulting the state-specific CASSCF wave functions of the ground and IVCT states and describing the crossing between them.

The charge values on both Fe atoms for the ground and IVCT states at each point of the electron transfer process are computed by means of the LoProp approach.⁴⁰ We define the so-called “electronic-sphere status” as a measure of the adaptation of the molecular orbitals in terms of an effective Fe charge

$$Q_x^{Fe} = (1 - x)q_{GS}^{Fe} + xq_{IVCT}^{Fe}$$

where x corresponds to the weight on the IVCT. Hence, the reported “electronic-sphere status” of a particular Fe atom is the weighted average of its atomic charge among the two states involved in the electron transfer, using the same distribution of weight employed in the CASSCF orbital optimization step.

The analysis of the electronic reorganization cannot be done by direct comparison of the delocalized orbitals of the ground and IVCT states obtained in the CASSCF step. Two equivalent sets of MOs can have morphologically different orbitals due to the presence of redundant orbital rotations that leave the CASSCF energy unchanged. For this reason, the absolute overlap of two equivalent versions of formally the same orbital can be lower than unity, reflecting an artificial change in morphology. Therefore, it is imperative to apply beforehand a common constraint over both sets of MOs. We have chosen one of the Kekulé structures of $Fe_a^{III}Fe_b^{II}LH$ (Figure S1) to build a reference space to project the

CASSCF orbitals into valence-bond like orbitals, the so-called localization *a posteriori*.^{41–43} The localization procedure is applied with the DOLO code included in the CASDI package.⁴⁴ By using the same localization scheme for the ground and IVCT MOs, we generate local orbitals that can be compared one-to-one unequivocally. Figure S2 shows the overlap values for all the inactive and active orbitals of the $\text{Fe}_a^{\text{III}}\text{Fe}_b^{\text{II}}\text{LH}$ compound.

Since the $\text{Fe}_a^{\text{III}}\text{Fe}_b^{\text{II}}\text{LH}$ molecule is relatively large, it is computationally too expensive to perform the complete active space second-order perturbation theory (CASPT2)⁴⁵ step over the complete space of the system (455 electrons in 816 MO). Therefore, by means of the localization of the MO set, we remove the less polarizable orbitals from the CASPT2 treatment and reduce its computational cost with a negligible loss of accuracy. Table S1 shows the exact distribution of the different orbitals types along the frozen, inactive, active, secondary and virtual spaces. We perform the CASPT2 calculations with the default IPEA value of 0.25 hartree and an imaginary shift factor of 0.20 hartree to minimize the intruder state problem.⁴⁶ We take profit of the Cholesky decomposition of the integrals to reduce the computational cost of working with this relatively big molecule.⁴⁷ The electronic structure calculations are performed using the MOLCAS 7 package.⁴⁸ The basis set scheme $(21s15p10d6f)/[6s5p4d2f]$ is used for Fe, $(14s9p4d)/[4s3p1d]$ for O and N atoms, $(14s9p)/[3s2p]$ for C and $(8s)/[2s]$ for H. All basis sets are of the ANO-RCC type.^{49,50}

RESULTS AND DISCUSSION

Figure 3 shows the energetic profile of the electronic ground state (blue) and the IVCT state (orange) as a function of the electronic reorganization triggered by the intramolecular electron transfer in the $\text{Fe}_a^{\text{III}}\text{Fe}_b^{\text{II}}\text{LH}$ compound. The molecular geometry is fixed along the curves and each set of points, for a given degree of electronic reorganization, is the result of a single CASSCF calculation with a single set of MOs (see Methods). The set of MOs is optimized with a particular distribution of weights over the eight lowest HS electronic states. By increasing the weight on the IVCT from 0 % to 100 % in the orbital optimization process, the electron density (or electronic-sphere) gradually adapts to the charge transfer configuration and hence, we virtually control the electronic reorganization triggered by the

IVCT.

The point of the curve at 0% of electronic reorganization corresponds to the state-specific CASSCF result of the ground state, meaning that the weight of the calculation is completely placed on the $\text{Fe}_a^{\text{III}}/\text{Fe}_b^{\text{II}}$ state. Following the variational principle, the energy value of the ground state at 0% is the best estimate that we can offer at this level of theory and accordingly, it is the absolute minimum of that curve. As the electron-sphere adapts to the IVCT ($\text{Fe}_a^{\text{II}}/\text{Fe}_b^{\text{III}}$), the absolute energy of the ground state becomes gradually higher while the IVCT state lowers in energy. Around 55% of electronic reorganization, both states cross and the character of the wave functions becomes strongly mixed. The identification of the states is not reliable in the degeneracy zones. Thus, these crossings are qualitatively represented in [Figure 3](#) with black dotted lines that do not represent the actual energy curves. Nonetheless, it is possible to jump over the crossing to a zone of non-degeneracy. Around 60% of reorganization, the weight on the IVCT is large enough to become the lowest electronic state, turning the initial fundamental state into an excited one. This inversion of spectroscopy is remarkable as it is a pure electronic phenomenon induced exclusively by the electronic reorganization and will be discussed in detail further below. Finally, at 100% of electronic reorganization, the IVCT energy corresponds to the state-specific CASSCF result for this state. This is the best description for the IVCT state at this level of theory and therefore, it is the absolute minimum energy of this state, in agreement with the variational principle.

The atomic charges of Fe_a and Fe_b are constant along the curve of each electronic state in [Figure 3](#). Therefore, the character of the diabatic states is unaltered by the electronic reorganization. The calculated charges for the Fe_a/Fe_b pair are 1.3/2.4 in the ground state and 2.3/1.4 in the IVCT state, clearly proving the transfer of one electron between the two metal centres. However, the energetics between these two states vary dramatically as a function of the electronic reorganization and therefore, the price to pay to transfer an electron from one metal centre to the other is largely affected by λ_e . The top part of [Figure 3](#) represents the “electronic-sphere status”, which is a measure of the electronic reorganization (see Methods). The charge distribution over the bi-iron core manifests the adaptation state of the electronic-sphere, linearly changing from a complete adaptation to

the $\text{Fe}_a^{\text{III}}/\text{Fe}_b^{\text{II}}$ arrangement at 0% of IVCT weight to the final $\text{Fe}_a^{\text{II}}/\text{Fe}_b^{\text{III}}$ at 100%. The linear behaviour of the “electronic-sphere status” is a consequence of the linear IVCT weight variation that we impose over the MOs. At the crossing zone ($\sim 55\%$), the “electronic-sphere status” shows that the electronic-sphere is in equilibrium to an equal distribution of charge over the Fe centres. This situation corresponds to the mono-valence domain of the $\text{Fe}_a^{\text{III}}\text{Fe}_b^{\text{II}}\text{LH}$ compound and confirms that the delocalization of the unpaired electron over the two iron centres is less favoured than both mixed-valence configurations, justifying the electron-trapped character of $\text{Fe}_a^{\text{III}}\text{Fe}_b^{\text{II}}\text{LH}$.

The crossing of states between the ground and IVCT states is a critical feature of **Figure 3**. It has a similar shape to Marcus’ model (**Figure 1**) with two minima close in energy separated by a potential barrier. However, the present inversion of spectroscopy is solely caused by pushing the optimization of the orbitals specifically to the charge transfer state and thus, only involves electronic reorganization, clearly demonstrating the major impact that λ_e can have. In a similar fashion to Marcus’ theory, where solvent molecules configurations are modified, the electronic structure fluctuates and triggers the electron transfer phenomenon at a given weight. The energetic cost of the IVCT excitation without any cooperation of the electronic-sphere (0%), the so-called rigid electron transfer, is 12.57 eV. The rigid IVCT is in a sense equivalent to a Koopmans’ ion state, the theoretical final state of an ultra-fast ionization.⁵¹⁻⁵⁴ This state is obtained by removing one electron from one orbital of the neutral species without taking into account the adaptation of other electrons (*i.e.* excluding electron correlation), following the prescription of Koopmans’ theorem.²³ The highly constrained rigid IVCT excitation is drastically affected by the electronic reorganization of the N-electron system. The adaptation of the full-electronic structure accounts for $\lambda_e = 11.74$ eV, a large amount that compensates the major part of the cost of the rigid IVCT. It must be noted that the calculated 12.57 and 11.74 eV values are upper bound limits of the rigid electron transfer and λ_e quantities, respectively. The hole/particle optimization is expected to lower both of them, but it is not present to maintain a coherent definition of the IVCT weight in **Figure 3**. The IVCT energy at 0% does not include any optimization of the MOs losing and gaining the electron.

The energy difference between the ground state in its equilibrated electronic-sphere (0%)

and the IVCT state in its equilibrated electronic-sphere (100 %) is 0.84 eV (Table 1). This result is in very good agreement with the experimental value of 0.98 eV for the light-induced IVCT on $\text{Fe}_a^{\text{III}}\text{Fe}_b^{\text{II}}\text{LH}$ ⁵⁵ and other very similar bi-iron mixed valence compounds.^{56,57} In contrast, the result obtained for the IVCT transition based on a state-average (SA) CASSCF calculation is 3.70 eV, too large a value despite being a strategy with many advantages for excited state calculations.⁵⁸ The SA-CASSCF energy corresponds to the vertical energy difference between the ground and IVCT states using a MO set optimized for all eight electronic states with an equal weight (totalling 37.5 % for the IVCT). This characteristic of state-average calculations is simultaneously their major strength and weakness, because working with an evenly balanced set of MOs eases the convergence of excited states calculations and ensures the orthogonality of the states, but it also conditions its application to ensembles of states that are relatively similar in nature. In the present case, the average of states with an opposite character ($\text{Fe}_a^{\text{III}}/\text{Fe}_b^{\text{II}}$ and $\text{Fe}_a^{\text{II}}/\text{Fe}_b^{\text{III}}$) is *not* well suited to describe either of them.

One way to verify the estimates for the IVCT transition obtained at the CASSCF level is to apply a perturbation treatment on top of the CASSCF wave function by means of the CASPT2 method. The lower the size of the CASPT2 perturbation correction to the wave function, the better the quality of the CASSCF reference. The IVCT transition energy obtained at the CASPT2 level from the state-specific reference is 0.89 eV (Table 1). This result incorporates a small perturbation correction to the wave function for both states (< 25 %), resulting in a small improvement over the CASSCF energy. Therefore, all the electronic dominant contributions are already present at the CASSCF level by using two different sets of orbitals. As expected, the quality of the IVCT transition energy does not benefit from the dynamical correlation treatment. However, the situation is the opposite for the state-average CASSCF reference. In that case, the resulting CASPT2 is unreliable due to a perturbation correction to the wave function larger than 80 %. This huge correction reflects the deep shortcomings of the SA-CASSCF reference.

The role of the set of MOs (or electronic-sphere) is generally underestimated, but the nature of the orbitals can be determinant in describing magnetic and spectroscopic phenomena.^{39,59,60} In the present case, allowing the orbitals to adapt to a specific electronic state

not only improves dramatically the IVCT energy of the $\text{Fe}_a^{\text{III}}\text{Fe}_b^{\text{II}}\text{LH}$ compound, but also empowers the inspection of changes induced by the electron transfer in the electronic structure. Since the size of the active space is constant along the curves of [Figure 3](#), the amount of electron correlation treated at the CASSCF level can also be considered constant and not affected by the IVCT weight. All electronic reorganization effects are described by single excitations incorporated in the adapted orbitals, which can be visualized and analysed. It must be noted that, in principle, similar improvements to the estimate of the IVCT transition energy could also be obtained by using better wave functions than the present CAS[11,10]SCF one. Larger active spaces could result in energies of the ground and IVCT states closer to their minimum value in [Figure 3](#) due to the larger amount of electron correlation treated in the wave function, in the form of an increased number of configuration state functions. Nonetheless, the capacity of analysing the response of the N-electron system to the electron transfer would be lost for larger active spaces, as the electronic reorganization effects would not be reflected in the orbitals. Since a larger CAS can incorporate the single excitations related to electronic reorganization in the wave function rather than in the orbitals, the energy values will be less dependent on the distribution of weight among the orbitals. Moreover, achieving the same level of accuracy obtained with the minimal CAS plus adapted orbitals would require the inclusion of the full orbital relaxation by means of single excitations in the CAS, involving a number of active orbitals that goes beyond the present computational limits. Therefore, the proposed strategy proves to not only be a cheaper solution to get accurate energetic estimates, but also a more powerful method to describe and understand electron transfer processes.

The electronic reorganization caused by the IVCT is quantified through the overlap between each orbital of the ground state and its counterpart of the IVCT state (S_{ET}). An overlap value of 1.00 means that both orbitals are strictly identical, and smaller overlaps indicate larger differences between them. To obtain meaningful S_{ET} values it is necessary to localize the orbitals of the ground and IVCT states by a projection over the same valence-bond like space (see Methods). This unitary transformation leaves the total N-electron wave function unaltered and generates local orbitals with a well defined character (*i.e.* σ , π or n). The local orbitals of the ground state can be paired unequivocally with their double

in the IVCT state and thus, we can evaluate the effect induced exclusively by the electron transfer. The S_{ET} values obtained for all orbitals are large, over 0.9000 (Figure S2), indicating that they are not deeply changed. Table 2 lists the few orbitals that have an overlap markedly lower than unity (< 0.9950) and thus, concentrate the major effects of electronic reorganization. Both Fe centres suffer an equal amount of reorganization. The expansion and contraction of the two Fe($3d-t_{2g}$) orbitals losing and gaining the transferred electron is opposite, but accounts for the same change of S_{ET} , 0.9915 and 0.9924 respectively (Figure 4). In spite of their spatial proximity to the transfer process, the $3d$ orbitals have a response to the IVCT significantly lower than the polarization induced in the O bridge and the pyrimidinic N coordinated to Fe_b. Surprisingly, all the π and n orbitals of those two atoms have overlaps lower than 0.9900. In the coordination shell of the bi-iron core, the strength of the induced polarization decays in the Fe_a \leftarrow Fe_b sense. One example is the S_{ET} value of the n orbitals that varies from 0.96 for the pyrimidinic N of Fe_b, to 0.98 for the O bridge and 0.99 for the N atoms of Fe_a (Figure 4). The fact that Fe_a has two pyrimidinic N atoms capable of adapting to the electron transfer, instead of only one for Fe_b, could justify the smaller individual alteration observed around the Fe_a centre. Moreover, the π orbitals are more polarized than the n orbitals located around the same atom. Since the adaptation of the n orbitals is limited, their polarization cannot follow freely the electric dipole field induced by the IVCT and instead, they tilt under the constraints of their environment reducing the repulsion with the δ^- charge on Fe_a.

CONCLUSIONS

The IVCT of the Fe_a^{III}Fe_b^{II}LH compound (Figure 2) involves two electronic states with an opposite charge distribution over the Fe centres, the Fe_a^{III}/Fe_b^{II} ground state and the Fe_a^{II}/Fe_b^{III} IVCT state. Such rearrangement of charge induces a response effect on the ensemble of electrons that must be properly treated to obtain an accurate description of the IVCT phenomenon, the so-called electronic reorganization. We developed and applied a computational strategy based on state-specific CASSCF wave functions that fulfils this requirement by including the complete adaptation of the molecular orbitals to each electronic state involved

in the electron transfer. The computed IVCT transition energy of the $\text{Fe}_a^{\text{III}}\text{Fe}_b^{\text{II}}\text{LH}$ compound is 0.89 eV, in very good agreement with the experimental value of 0.98 eV. We quantify the contribution of the electronic-sphere to the reorganization energy of the IVCT transition to be $\lambda_e = 11.74$ eV, having a major impact on the energetics of the electron transfer process of the $\text{Fe}_a^{\text{III}}\text{Fe}_b^{\text{II}}\text{LH}$ complex (Figure 3). This result reflects the critical role of the molecular orbitals in describing phenomena that induce large electronic reorganization. Moreover, the electronic reorganization alone is capable of producing the crossing of the ground and IVCT states, being a pure electronic phenomena that generates a metastable IVCT state and having the same effect as the reorganization energy in Marcus' model (Figure 1). In the present case, the large energetic effect of λ_e is produced by a relatively small adaptation of the valence electrons in the first-coordination shell and Fe centres, which become polarized following the dipole induced by the IVCT transition (Table 2). Even though the Fe(3d) electrons are spatially closer to the transfer process, the electronic reorganization is stronger in the pyrimidinic N coordinated to Fe_b and decays progressively through the O bridge and towards the N coordinated to Fe_a (Figure 4). The inversion of spectroscopy induced by λ_e is characteristic of the light-induced IVCT, which triggers the electron transfer. On the other hand, the pH-induced electron transfer generates a relatively slow response of the nuclei to which the electrons get adapted instantaneously, in closer agreement to the standard Marcus' model or its extension for PCET including Morse potentials.¹⁹ Thus, the effect of the electronic-sphere will be more significant for the light-induced electron transfer, whereas the inner- and outer-sphere will be determinant for the pH-induced process.

ACKNOWLEDGMENTS

Financial support has been provided by the Agence Nationale de la Recherche (ANR) (Project ANR-2010-BLAN-703), the excellence network Chemistry of Complex Systems (LabEx CSC, ANR-10-LABX-0026_CSC) and the Spanish and Catalan administrations (CTQ 2011-23140 and 2009SGR462). C.A. is grateful to the University of Strasbourg for the possibility of staying as an Invited Professor in 2013.

Additional Supporting Information may be found in the online version of this article.

References

1. T. J. Meyer, M. H. V. Huynh, and H. H. Thorp, *The Possible Role of Proton-Coupled Electron Transfer (PCET) in Water Oxidation by Photosystem II*, *Angew. Chem. Int. Ed.* **46**, 5284–5304 (2007).
2. I. Belevich, M. I. Verkhovsky, and M. Wikström, *Proton-coupled electron transfer drives the proton pump of cytochrome c oxidase*, *Nature* **440**, 829 (2006).
3. J. C. Genereux and J. K. Barton, *Mechanisms for DNA Charge Transport*, *Chem. Rev.* **110**, 1642 (2010).
4. J. L. Dempsey, A. J. Esswein, D. R. Manke, J. Rosenthal, J. D. Soper, and D. G. Nocera, *Molecular Chemistry of Consequence to Renewable Energy*, *Inorg. Chem.* **44**, 6879 (2005).
5. D. G. Nocera, *Chemistry of Personalized Solar Energy*, *Inorg. Chem.* **48**, 10001 (2009).
6. M. D. Ward, *Photo-induced electron and energy transfer in non-covalently bonded supramolecular assemblies*, *Chem. Soc. Rev.* **26**, 365 (1997).
7. F.-Y. Wu and Y.-B. Jiang, *p-Dimethylaminobenzamide as an ICT dual fluorescent neutral receptor for anions under proton coupled electron transfer sensing mechanism*, *Chem. Phys. Lett.* **355**, 438 (2002).
8. M. Grätzel, *Photoelectrochemical cells*, *Nature* **414**, 338 (2001).
9. R. A. Marcus, *Chemical and Electrochemical Electron-Transfer Theory*, *Annu. Rev. Phys. Chem.* **15**, 155 (1964).
10. R. A. Marcus, *Electron transfer reactions in chemistry. Theory and experiment*, *Rev. Mod. Phys.* **65**, 599 (1993).
11. M. D. Newton, in *Electron Transfer in Chemistry*, edited by V. Balzani (Wiley-VCH Verlag GmbH, 2008), p. 2–63.

12. J. M. Mayer, *PROTON-COUPLED ELECTRON TRANSFER: A Reaction Chemist's View*, Annu. Rev. Phys. Chem. **55**, 363 (2004).
13. D. R. Weinberg, C. J. Gagliardi, J. F. Hull, C. F. Murphy, C. A. Kent, B. C. Westlake, A. Paul, D. H. Ess, D. G. McCafferty, and T. J. Meyer, *Proton-Coupled Electron Transfer*, Chem. Rev. **112**, 4016 (2012).
14. A. L. Feig and S. J. Lippard, *Reactions of Non-Heme Iron(II) Centers with Dioxygen in Biology and Chemistry*, Chem. Rev. **94**, 759 (1994).
15. E. I. Solomon, T. C. Brunold, M. I. Davis, J. N. Kemsley, S.-K. Lee, N. Lehnert, F. Neese, A. J. Skulan, Y.-S. Yang, and J. Zhou, *Geometric and Electronic Structure/Function Correlations in Non-Heme Iron Enzymes*, Chem. Rev. **100**, 235 (2000).
16. E. Gouré, G. Thiabaud, M. Carboni, N. Gon, P. Dubourdeaux, R. Garcia-Serres, M. Clémancey, J.-L. Oddou, A. Y. Robin, L. Jacquamet, L. Dubois, G. Blondin, and J.-M. Latour, *Reversible (De)protonation-Induced Valence Inversion in Mixed-Valent Diiron(II,III) Complexes*, Inorg. Chem. **50**, 6408 (2011).
17. R. Balasubramanian, G. Blondin, J. C. Canales, C. Costentin, J.-M. Latour, M. Robert, and J.-M. Savéant, *Proton-Coupled Intervalence Charge Transfer: Concerted Processes*, J. Am. Chem. Soc. **134**, 1906 (2012).
18. C. Costentin, M. Robert, and J.-M. Savéant, *Concerted Proton-Electron Transfers: Electrochemical and Related Approaches*, Accounts Chem. Res. **43**, 1019 (2010).
19. C. Costentin, M. Robert, J.-M. Savéant, and C. Tard, *Breaking Bonds with Electrons and Protons. Models and Examples*, Accounts Chem. Res. (2013).
20. F. Remacle and R. D. Levine, *An electronic time scale in chemistry*, Proc. Natl. Acad. Sci. U.S.A. **103**, 6793 (2006).
21. A. I. Kuleff, S. Lünemann, and L. S. Cederbaum, *Electron-correlation-driven charge migration in oligopeptides*, Chem. Phys. **414**, 100 (2013).

22. M. Born and R. Oppenheimer, *Zur Quantentheorie der Molekeln*, Ann. Phys. (Berlin) **389**, 457–484 (1927).
23. A. Szabo, *Modern Quantum Chemistry: Introduction to Advanced Electronic Structure Theory* (Courier Dover Publications, 1996).
24. C. J. Cramer and D. G. Truhlar, *Density functional theory for transition metals and transition metal chemistry*, Phys. Chem. Chem. Phys. **11**, 10757 (2009).
25. E. Runge and E. K. U. Gross, *Density-Functional Theory for Time-Dependent Systems*, Phys. Rev. Lett. **52**, 997 (1984).
26. M. Marques, C. Ullrich, F. Nogueira, A. Rubio, K. Burke, and E. Gross, *Time-Dependent Density Functional Theory*, vol. 706 of *Lecture Notes in Physics* (Springer-Verlag, New York, 2006).
27. M. E. Casida, *Time-dependent density-functional theory for molecules and molecular solids*, J. Mol. Struct.-THEOCHEM **914**, 3 (2009).
28. C. Faber, I. Duchemin, T. Deutsch, and X. Blase, *Many-body Green's function study of coumarins for dye-sensitized solar cells*, Phys. Rev. B **86**, 155315 (2012).
29. A. J. Cohen, P. Mori-Sánchez, and W. Yang, *Insights into Current Limitations of Density Functional Theory*, Science **321**, 792 (2008).
30. Q. Wu and T. Van Voorhis, *Direct optimization method to study constrained systems within density-functional theory*, Phys. Rev. A **72**, 024502 (2005).
31. Q. Wu and T. Van Voorhis, *Constrained Density Functional Theory and Its Application in Long-Range Electron Transfer*, J. Chem. Theory Comput. **2**, 765 (2006).
32. B. Kaduk, T. Kowalczyk, and T. Van Voorhis, *Constrained Density Functional Theory*, Chem. Rev. **112**, 321 (2012).
33. Y. Lu, R. Quardokus, C. S. Lent, F. Justaud, C. Lapinte, and S. A. Kandel, *Charge Localization in Isolated Mixed-Valence Complexes: An STM and Theoretical Study*, J. Am. Chem. Soc. **132**, 13519 (2010).

34. R. C. Quardokus, Y. Lu, N. A. Wasio, C. S. Lent, F. Justaud, C. Lapinte, and S. A. Kandel, *Through-Bond versus Through-Space Coupling in Mixed-Valence Molecules: Observation of Electron Localization at the Single-Molecule Scale*, *J. Am. Chem. Soc.* **134**, 1710 (2012).
35. B. O. Roos, P. R. Taylor, and P. E. M. Siegbahn, *A complete active space SCF method (CASSCF) using a density matrix formulated super-CI approach*, *Chem. Phys.* **48**, 157 (1980).
36. S. Chardon-Noblat, O. Horner, B. Chabut, F. Avenier, N. Debaecker, P. Jones, J. Pécaut, L. Dubois, C. Jeandey, J.-L. Oddou, A. Deronzier, and J.-M. Latour, *Spectroscopic and Electrochemical Characterization of an Aqua Ligand Exchange and Oxidatively Induced Deprotonation in Diiron Complexes*, *Inorg. Chem.* **43**, 1638 (2004).
37. P.-Å. Malmqvist and B. O. Roos, *The CASSCF state interaction method*, *Chem. Phys. Lett.* **155**, 189 (1989).
38. A. Domingo, M. À. Carvajal, C. de Graaf, K. Sivalingam, F. Neese, and C. Angeli, *Metal-to-metal charge-transfer transitions: reliable excitation energies from ab initio calculations*, *Theor. Chem. Acc.* **131**, 1 (2012).
39. B. Meyer, A. Domingo, T. Krahl, and V. Robert, *Charge Transfer Processes: the Role of Optimized Molecular Orbitals*, *Dalton Trans.* (2014).
40. L. Gagliardi, R. Lindh, and G. Karlström, *Local properties of quantum chemical systems: The LoProp approach*, *J. Chem. Phys.* **121**, 4494 (2004).
41. S. F. Boys, *Construction of Some Molecular Orbitals to Be Approximately Invariant for Changes from One Molecule to Another*, *Rev. Mod. Phys.* **32**, 296 (1960).
42. C. Angeli, G. Del Re, and M. Persico, *Quasi-bond orbitals from maximum-localization hybrids for ab initio CI calculations*, *Chem. Phys. Lett.* **233**, 102 (1995).
43. J.-P. Malrieu, N. Guihéry, C. J. Calzado, and C. Angeli, *Bond electron pair: Its relevance and analysis from the quantum chemistry point of view*, *J. Comput. Chem.* **28**, 35–50 (2007).

44. N. Ben Amor and D. Maynau, *Size-consistent self-consistent configuration interaction from a complete active space*, Chem. Phys. Lett. **286**, 211 (1998).
45. K. Andersson, P.-Å. Malmqvist, and B. O. Roos, *Second-order perturbation theory with a complete active space self-consistent field reference function*, J. Chem. Phys. **96**, 1218 (1992).
46. N. Forsberg and P.-Å. Malmqvist, *Multiconfiguration perturbation theory with imaginary level shift*, Chem. Phys. Lett. **274**, 196 (1997).
47. F. Aquilante, P.-Å. Malmqvist, T. B. Pedersen, A. Ghosh, and B. O. Roos, *Cholesky Decomposition-Based Multiconfiguration Second-Order Perturbation Theory (CD-CASPT2): Application to the Spin-State Energetics of CoIII(diiminato)(NPh)*, J. Chem. Theory Comput. **4**, 694 (2008).
48. F. Aquilante, L. De Vico, N. Ferré, G. Ghigo, P.-Å. Malmqvist, P. Neogrády, T. B. Pedersen, M. Pitoňák, M. Reiher, B. O. Roos, L. Serrano-Andrés, M. Urban, V. Veryazov, and R. Lindh, *MOLCAS 7: The Next Generation*, J. Comput. Chem. **31**, 224–247 (2010).
49. B. O. Roos, R. Lindh, P.-Å. Malmqvist, V. Veryazov, and P.-O. Widmark, *Main Group Atoms and Dimers Studied with a New Relativistic ANO Basis Set*, J. Phys. Chem. A **108**, 2851 (2004).
50. B. O. Roos, R. Lindh, P.-Å. Malmqvist, V. Veryazov, and P.-O. Widmark, *New Relativistic ANO Basis Sets for Transition Metal Atoms*, J. Phys. Chem. A **109**, 6575 (2005).
51. G. Sansone, T. Pfeifer, K. Simeonidis, and A. I. Kuleff, *Electron Correlation in Real Time*, ChemPhysChem **13**, 661–680 (2012).
52. A. I. Kuleff, S. Lünemann, and L. S. Cederbaum, *Ultrafast reorganization of the hole charge created upon outer-valence ionization of porphyrins*, Chem. Phys. **399**, 245 (2012).

53. A. D. Dutoi, K. Gokhberg, and L. S. Cederbaum, *Time-resolved pump-probe spectroscopy to follow valence electronic motion in molecules: Theory*, Phys. Rev. A **88**, 013419 (2013).
54. A. I. Kuleff and L. S. Cederbaum, *Ultrafast correlation-driven electron dynamics*, J. Phys. B **47**, 124002 (2014).
55. G. Blondin and J.-M. Latour, Private Communication (2013).
56. A. S. Borovik and L. Que, *Models for the iron(II)iron(III) and iron(II)iron(II) forms of iron-oxo proteins*, J. Am. Chem. Soc. **110**, 2345 (1988).
57. A. S. Borovik, V. Papaefthymiou, L. F. Taylor, O. P. Anderson, and L. Que, *Models for iron-oxo proteins. Structures and properties of FeIIFeIII, ZnIIFeIII, and FeIIGaIII complexes with (.mu.-phenoxo)bis(.mu.-carboxylato)dimetal cores*, J. Am. Chem. Soc. **111**, 6183 (1989).
58. L. González, D. Escudero, and L. Serrano-Andrés, *Progress and Challenges in the Calculation of Electronic Excited States*, ChemPhysChem **13**, 28–51 (2012).
59. C. Angeli, *On the nature of the $\pi \rightarrow \pi^*$ ionic excited states: The V state of ethene as a prototype*, J. Comput. Chem. **30**, 1319–1333 (2009).
60. C. Angeli and C. J. Calzado, *The role of the magnetic orbitals in the calculation of the magnetic coupling constants from multireference perturbation theory methods*, J. Chem. Phys. **137**, 034104 (2012).

Figure 1: Marcus’ model: adiabatic energy curves and relevant quantities (reorganization energy (λ), standard free energy (ΔG^0) and activation energy (E_a)) as a function of the quantity of charge transferred (Δe) for the electron transfer reaction $M_a^{n+1} + M_b^n \rightarrow M_a^n + M_b^{n+1}$.

Figure 2: Molecular structure of the $[\text{Fe}^{\text{III}}\text{Fe}^{\text{II}}(\text{NH}_2\text{-L})(\text{mpdp})]^{2+}$ ($\text{mpdp}^{2-} = \text{m-phenylenedipropionate}$) bio-mimetic compound derived from X-ray data.¹⁷

Figure 3: CASSCF energy profile of the ground state (blue) and the IVCT state (orange) as a function of the electronic reorganization induced by the IVCT in the $\text{Fe}_a^{\text{III}}\text{Fe}_b^{\text{II}}\text{LH}$ compound. Intra-metallic d-d transitions on Fe are plotted in grey. Inset top-left: complete curves including the rigid IVCT and the following electronic reorganization (λ_e). Top: the “electronic-sphere status”, a measure of λ_e in terms of the effective charge of Fe_a (grey) and Fe_b (black) to which the electronic-sphere is adapted (see Methods).

Figure 4: Electronic reorganization induced by the IVCT of the $\text{Fe}_a^{\text{III}}\text{Fe}_b^{\text{II}}\text{LH}$ compound on some representative local orbitals. The shape of each orbital is depicted for the ground state (dotted) and for the IVCT state (solid). The arrows in the orbitals indicate the induced polarization by the IVCT. The background represents the electric field of the induced dipole.

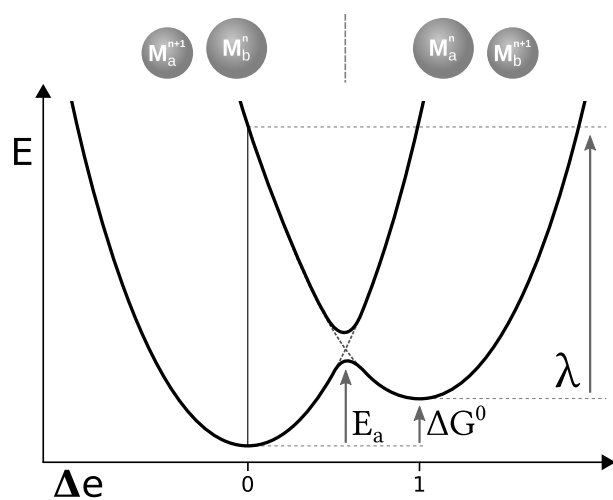


Figure 1

A. Domingo, C. Angeli, C. de Graaf, V. Robert
 J. Comput. Chem.

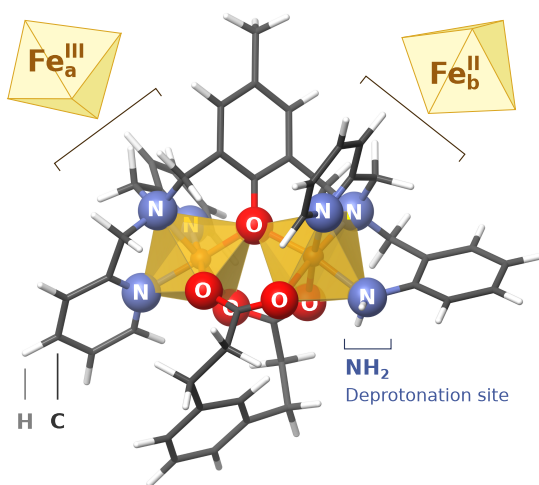


Figure 2

A. Domingo, C. Angeli, C. de Graaf, V. Robert
 J. Comput. Chem.

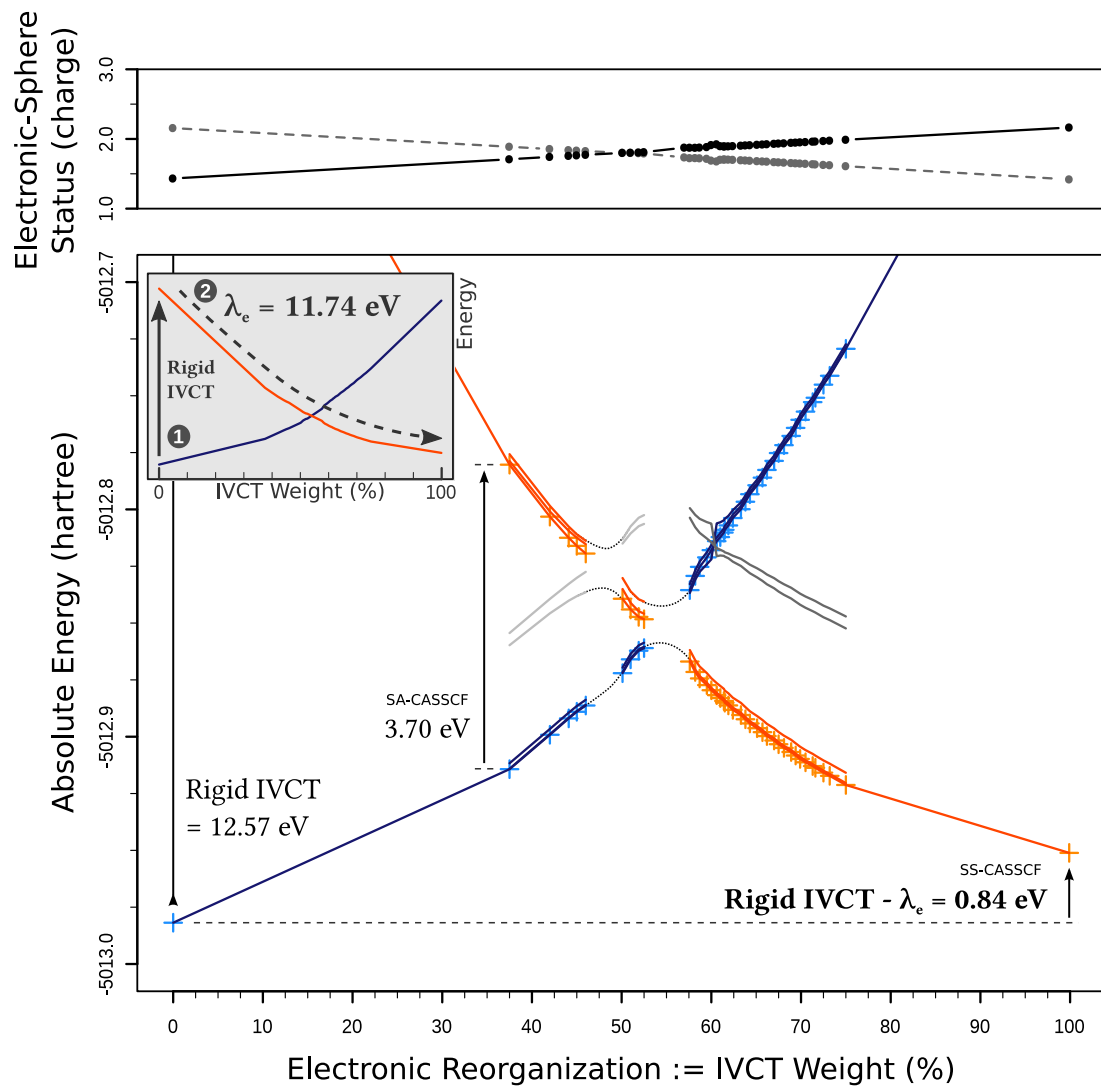


Figure 3
 A. Domingo, C. Angeli, C. de Graaf, V. Robert
 J. Comput. Chem.

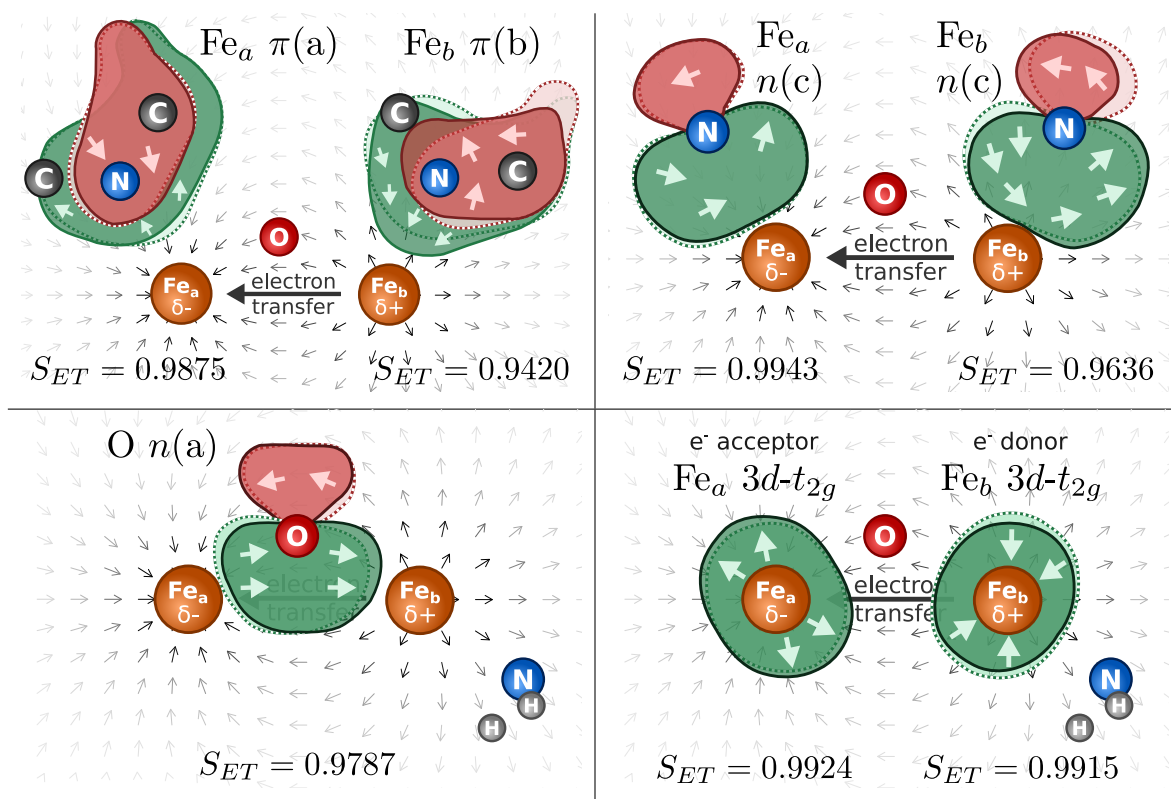


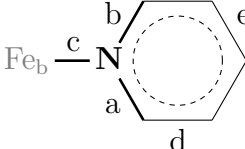
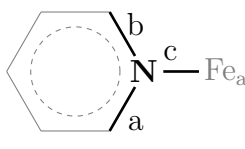
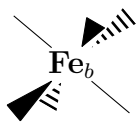
Figure 4
 A. Domingo, C. Angeli, C. de Graaf, V. Robert
 J. Comput. Chem.

Table 1: Comparison of the charge transfer energy obtained from the state-specific and state-average calculations of the $\text{Fe}_a^{\text{III}}\text{Fe}_b^{\text{II}}\text{LH}$ complex.

| State | MO | IVCT | CASPT2 | | CASSCF |
|-------|----------|---------|----------------------|-----------|-----------|
| | Set | Weight | Correc. ^a | IVCT (eV) | IVCT (eV) |
| GS | Specific | 0.0 % | 21 % | 0.89 | 0.84 |
| IVCT | Specific | 100.0 % | 12 % | | |
| GS | Average | 37.5 % | > 80 % | × | 3.70 |
| IVCT | | 37.5 % | > 80 % | | |

^a The perturbation correction to the wave function of the CASPT2 result.

Table 2: Local orbitals of $\text{Fe}_a^{\text{III}}\text{Fe}_b^{\text{II}}\text{LH}$ with an S_{ET} overlap lower than 0.9950. Orbitals marked with stars are depicted in [Figure 4](#).

| Localization | Local Orbital | S_{ET} Overlap |
|---|---------------------|------------------|
|  | $\pi(\text{a})$ | 0.9184 |
| | * $\pi(\text{b})$ * | 0.9420 |
| | * $n(\text{c})$ * | 0.9636 |
| | $\pi(\text{d})$ | 0.9782 |
| | $\pi(\text{e})$ | 0.9926 |
|  | * $\pi(\text{a})$ * | 0.9875 |
| | $\pi(\text{b})$ | 0.9910 |
| | * $n(\text{c})$ * | 0.9943 |
|  | * $n(\text{a})$ * | 0.9787 |
| | $n(\text{b})$ | 0.9827 |
|  | * $3d-t_{2g}$ * | 0.9915 |
| | $3d-e_g$ | 0.9932 |
| | $3d-e_g$ | 0.9935 |
|  | * $3d-t_{2g}$ * | 0.9924 |
| | $3d-e_g$ | 0.9926 |
| | $3d-e_g$ | 0.9942 |